Search for Dark Matter Annihilation Signals from the Fornax Galaxy Cluster with H.E.S.S.

H.E.S.S. Collaboration: A. Abramowski[1], F. Acero[2], F. Aharonian[3,4,5], A.G. Akhperjanian[6,5], G. Anton[7], A. Balzer[7], A. Barnacka[8,9], U. Barres de Almeida[10,*], Y. Becherini[11,12], J. Becker [13], B. Behera[14], K. Bernlöhr[3,15], E. Birsin[15], J. Biteau[12], A. Bochow[3], C. Boisson[16], J. Bolmont[17], P. Bordas[18], J. Brucker[7], F. Brun[12], P. Brun[9], T. Bulik[19], I. Büsching[20,13], S. Carrigan[3], S. Casanova[13], M. Cerruti[16], P.M. Chadwick[10], A. Charbonnier[17], R.C.G. Chaves[3], A. Cheesebrough[10], A.C. Clapson[3], G. Coignet[21], G. Cologna[14], J. Conrad[22], M. Dalton[15], M.K. Daniel[10], I.D. Davids[23], B. Degrange[12], C. Deil[3], H.J. Dickinson[22], A. Djannati-Ataï[11], W. Domainko[3], L.O'C. Drury[4], G. Dubus[24], K. Dutson[25], J. Dyks[8], M. Dyrda[26], K. Egberts[27], P. Eger[7], P. Espigat[11], L. Fallon[4], C. Farnier[2], S. Fegan[12], F. Feinstein[2], M.V. Fernandes[1], A. Fiasson[21], G. Fontaine[12], A. Förster[3], M. Füßling[15], Y.A. Gallant[2], H. Gast[3], L. Gérard[11], D. Gerbig[13], B. Giebels[12], J.F. Glicenstein[9], B. Glück[7], P. Goret[9], D. Göring[7], S. Häffner [7], J.D. Hague [3], D. Hampf[1], M. Hauser[14], S. Heinz[7], G. Heinzelmann[1], G. Henri[24], G. Hermann[3], J.A. Hinton[25], A. Hoffmann[18], W. Hofmann[3], P. Hofverberg[3], M. Holler[7], D. Horns[1], A. Jacholkowska[17], O.C. de Jager[20], C. Jahn[7], M. Jamrozy[28], I. Jung[7], M.A. Kastendieck[1], K. Katarzyński[29], U. Katz[7], S. Kaufmann[14], D. Keogh[10], D. Khangulyan[3], B. Khélifi[12], D. Klochkov[18], W. Kluźniak[8], T. Kneiske[1], Nu. Komin[21], K. Kosack[9], R. Kossakowski[21], H. Laffon[12], G. Lamanna[21], D. Lennarz[3], T. Lohse[15], A. Lopatin[7], C.-C. Lu[3], V. Marandon[11], A. Marcowith[2], J. Masbou[21], D. Maurin[17], N. Maxted[30], M. Mayer[7], T.J.L. McComb[10], M.C. Medina[9], J. Méhault[2], R. Moderski[8], E. Moulin[9], C.L. Naumann[17], M. Naumann-Godo[9], M. de Naurois[12], D. Nedbal[31], D. Nekrassov[3], N. Nguyen[1], B. Nicholas[30], J. Niemiec[26], S.J. Nolan[10], S. Ohm[32,25,3], E. de Oña Wilhelmi[3], B. Opitz[1,‡], M. Ostrowski[28], I. Oya[15], M. Panter[3], M. Paz Arribas[15], G. Pedaletti[14], G. Pelletier[24], P.-O. Petrucci[24], S. Pita[11], G. Pühlhofer[18], M. Punch[11], A. Quirrenbach[14], M. Raue[1], S.M. Rayner[10], A. Reimer[27], O. Reimer[27], M. Renaud[2], R. de los Reyes[3], F. Rieger[3,33], J. Ripken[22], L. Rob[31], S. Rosier-Lees[21], G. Rowell[30], B. Rudak[8], C.B. Rulten[10], J. Ruppel[13], V. Sahakian[6,5], D.A. Sanchez[3], A. Santangelo[18], R. Schlickeiser[13], F.M. Schöck[7], A. Schulz[7], U. Schwanke[15], S. Schwarzburg[18], S. Schwemmer[14], F. Sheidaei[11,20], J.L. Skilton[3], H. Sol[16], G.Spengler[15], Ł. Stawarz[28], R. Steenkamp[23], C. Stegmann[7], F. Stinzing[7], K. Stycz[7], I. Sushch[15,**], A. Szostek[28], J.-P. Tavernet[17], R. Terrier[11], M. Tluczykont[1], K. Valerius[7], C. van Eldik[3], G. Vasileiadis[2], C. Venter[20], J.P. Vialle[21], A. Viana[9,‡], P. Vincent[17], H.J. Völk[3], F. Volpe[3], S. Vorobiov[2], M. Vorster[20], S.J. Wagner[14], M. Ward[10], R. White[25], A. Wierzcholska[28], M. Zacharias[13], A. Zajczyk[8,2], A.A. Zdziarski[8], A. Zech[16], H.-S. Zechlin[1]

[†]bjoern.opitz@desy.de

[‡]aion.viana@cea.fr

[1]Universität Hamburg, Institut für Experimentalphysik, Luruper Chaussee 149, D 22761 Hamburg, Germany

[2]Laboratoire de Physique Théorique et Astroparticules, Université Montpellier 2, CNRS/IN2P3, CC 70, Place Eugène Bataillon, F-34095 Montpellier Cedex 5, France

[3]Max-Planck-Institut für Kernphysik, P.O. Box 103980, D 69029 Heidelberg, Germany

[4]Dublin Institute for Advanced Studies, 31 Fitzwilliam Place, Dublin 2, Ireland

[5]National Academy of Sciences of the Republic of Armenia, Yerevan

[6]Yerevan Physics Institute, 2 Alikhanian Brothers St., 375036 Yerevan, Armenia

[7]Universität Erlangen-Nürnberg, Physikalisches Institut, Erwin-Rommel-Str. 1, D 91058 Erlangen, Germany

[8]Nicolaus Copernicus Astronomical Center, ul. Bartycka 18, 00-716 Warsaw, Poland

[9]IRFU/DSM/CEA, CE Saclay, F-91191 Gif-sur-Yvette, Cedex, France

[10]University of Durham, Department of Physics, South Road, Durham DH1 3LE, U.K.

[11]Astroparticule et Cosmologie (APC), CNRS, Université Paris 7 Denis Diderot, 10, rue Alice Domon et Leonie Duquet, F-75205 Paris Cedex 13, France. Also at UMR 7164 (CNRS, Université Paris VII, CEA, Observatoire de Paris)

[12]Laboratoire Leprince-Ringuet, Ecole Polytechnique, CNRS/IN2P3, F-91128 Palaiseau, France

[13]Institut für Theoretische Physik, Lehrstuhl IV: Weltraum und Astrophysik, Ruhr-Universität Bochum, D 44780 Bochum, Germany

[14]Landessternwarte, Universität Heidelberg, Königstuhl, D 69117 Heidelberg, Germany

[15]Institut für Physik, Humboldt-Universität zu Berlin, Newtonstr. 15, D 12489 Berlin, Germany

[16]LUTH, Observatoire de Paris, CNRS, Université Paris Diderot, 5 Place Jules Janssen, 92190 Meudon, France

[17]LPNHE, Université Pierre et Marie Curie Paris 6, Université Denis Diderot Paris 7, CNRS/IN2P3, 4 Place Jussieu, F-75252, Paris Cedex 5, France

[18]Institut für Astronomie und Astrophysik, Universität Tübingen, Sand 1, D 72076 Tübingen, Germany

[19]Astronomical Observatory, The University of Warsaw, Al. Ujazdowskie 4, 00-478 Warsaw, Poland

[20]Unit for Space Physics, North-West University, Potchefstroom 2520, South Africa

[21]Laboratoire d'Annecy-le-Vieux de Physique des Particules, CNRS/IN2P3, 9 Chemin de Bellevue - BP 110 F-74941 Annecy-le-Vieux Cedex, France

[22]Oskar Klein Centre, Department of Physics, Royal Institute of Technology (KTH), Albanova, SE-10691

Abstract

The Fornax galaxy cluster was observed with the High Energy Stereoscopic System (H.E.S.S.) for a total live time of 14.5 hours, searching for very-high-energy (VHE, $E > 100$ GeV) γ-rays from dark matter (DM) annihilation. No significant signal was found in searches for point-like and extended emissions. Using several models of the DM density distribution, upper limits on the DM velocity-weighted annihilation cross-section $\langle \sigma v \rangle$ as a function of the DM particle mass are derived. Constraints are derived for different DM particle models, such as those arising from Kaluza-Klein and supersymmetric models. Various annihilation final states are considered. Possible enhancements of the DM annihilation γ-ray flux, due to DM substructures of the DM host halo, or from the *Sommerfeld* effect, are studied. Additional γ-ray contributions from internal bremsstrahlung and inverse Compton radiation are also discussed. For a DM particle mass of 1 TeV, the exclusion limits at 95% of confidence level reach values of $\langle \sigma v \rangle^{95\%\,\mathrm{C.L.}} \sim 10^{-23}$ cm^{3}s^{-1}, depending on the DM particle

Stockholm, Sweden

[23]University of Namibia, Department of Physics, Private Bag 13301, Windhoek, Namibia

[24]Laboratoire d'Astrophysique de Grenoble, INSU/CNRS, Université Joseph Fourier, BP 53, F-38041 Grenoble Cedex 9, France

[25]Department of Physics and Astronomy, The University of Leicester, University Road, Leicester, LE1 7RH, United Kingdom

[26]Instytut Fizyki Jądrowej PAN, ul. Radzikowskiego 152, 31-342 Kraków, Poland

[27]Institut für Astro- und Teilchenphysik, Leopold-Franzens-Universität Innsbruck, A-6020 Innsbruck, Austria

[28]Obserwatorium Astronomiczne, Uniwersytet Jagielloński, ul. Orla 171, 30-244 Kraków, Poland

[29]Toruń Centre for Astronomy, Nicolaus Copernicus University, ul. Gagarina 11, 87-100 Toruń, Poland

[30]School of Chemistry & Physics, University of Adelaide, Adelaide 5005, Australia

[31]Charles University, Faculty of Mathematics and Physics, Institute of Particle and Nuclear Physics, V Holešovičkách 2, 180 00 Prague 8, Czech Republic

[32]School of Physics & Astronomy, University of Leeds, Leeds LS2 9JT, UK

[33]European Associated Laboratory for Gamma-Ray Astronomy, jointly supported by CNRS and MPG

[*]supported by CAPES Foundation, Ministry of Education of Brazil

[**]supported by Erasmus Mundus, External Cooperation Window

model and halo properties. Additional contribution from DM substructures can improve the upper limits on $\langle\sigma v\rangle$ by more than two orders of magnitude. At masses around 4.5 TeV, the enhancement by substructures and the Sommerfeld resonance effect results in a velocity-weighted annihilation cross-section upper limit at the level of $\langle\sigma v\rangle^{95\%\,\mathrm{C.L.}} \sim 10^{-26}$ cm^{3}s^{-1}.

Subject headings: Gamma-rays : observations - Galaxy Cluster, Dark Matter, Fornax galaxy cluster

1. Introduction

Galaxy clusters are the largest virialized objects observed in the Universe. Their main mass component is dark matter (DM), making up about 80% of their total mass budget, with the remainder provided by intracluster gas and galaxies, at 15% and 5% respectively (see e.g Voit 2005). The DM halo distribution within galaxy clusters appears to be well reproduced by N-body numerical simulations for gravitational structure formation (Colafrancesco *et al.* 2006; Richtler *et al.* 2008; Schuberth *et al.* 2010; Voit 2005, and references therein). This may be in contrast to smaller systems like dwarf galaxies. For instance, disagreements between theoretical predictions and actual estimates of the DM halo profile from observations have been found in low surface brightness galaxies (McGaugh and de Blok 1998; Navarro 1998; de Blok 2010). Although such discrepancies may vanish at galaxy cluster scale, the influence of baryon infall in the DM gravitational potential can still flatten the DM density distribution in the inner regions of galaxy clusters (see, for instance, El-Zant *et al.* 2001).

The pair annihilation of weakly interacting massive particles (WIMP) constituting the DM halo is predicted to be an important source of non-thermal particles, including a significant fraction as photons covering a broad multiwavelength spectrum of emission (see, for instance, Bergstrom 2000; Colafrancesco *et al.* 2006). Despite the fact that galaxy clusters are located at much further distances than the dwarf spheroidal galaxies around the Milky Way, the higher annihilation luminosity of clusters make them comparably good targets for indirect detection of dark matter. The flux of γ-rays from WIMP DM annihilation in clusters of galaxies is possibly large enough to be detected by current γ-ray telescopes (Jeltema *et al.* 2009; Pinzke *et al.* 2009). Also standard astrophysical scenarios have been proposed for γ-ray emission (see e.g. Blasi *et al.* 2007, for a review), in particular, collisions of intergalactic cosmic rays and target nuclei from the intracluster medium. Despite these predictions, no significant γ-ray emission has been observed in local clusters by H.E.S.S. (Aharonian *et al.* 2009a,c), MAGIC (Aleksić *et al.* 2010a) and *Fermi*-

LAT (Ackermann *et al.* 2010a,b) collaborations. However, γ-rays of a different astrophysical emission processes have already been detected from some central radio galaxies in clusters (e.g. Aharonian *et al.* (2006a); Acciari *et al.* (2008); Aleksić *et al.* (2010b); Abdo *et al.* (2009)).

Following the absence of a signal, upper limits for a DM annihilation signal coming from galaxy clusters have been published by *Fermi*-LAT (Ackermann *et al.* 2010a) and MAGIC (Aleksić *et al.* 2010a) collaborations. Strong constraints on the annihilation cross-section of DM from the Fornax galaxy cluster have been put by the *Fermi*-LAT collaboration for DM particles masses up to 1 TeV from γ-ray selected in the 100 MeV - 100 GeV energy range. However many DM models show distinct features in the DM annihilation spectrum close to DM particle mass, such as monochromatic gamma-ray lines, sharp steps or cut-offs, as well as pronounced bumps. This could provide a clear distinction between an annihilation signal and a standard astrophysical signal (see, for instance, Bringmann *et al.* 2011)). These features are often referred as *smoking-gun* signatures. Such models can only be tested by satellite telescopes for DM particle masses up to a few hundreds of GeV. IACTs observation can provide well-complementary searches for such features at DM particle masses higher than a few hundreds of GeV .

This paper reports on the observation in VHE γ rays of the Fornax galaxy cluster (ACO S373) with the High Energy Stereoscopic System (H.E.S.S.). Interdependent constraints on several DM properties are derived from the data, such as the DM particle mass and annihilation cross-section. Different models of the DM density distribution of the cluster halo are studied. The paper is structured as follows. In Section 2 the Fornax galaxy cluster is described. The choice of Fornax for a DM analysis is motivated, based on the DM content and distribution inside the cluster. Section 3 presents the data analysis and results. Upper limits on the γ-ray flux for both standard astrophysical sources and DM annihilation are extracted in Section 4. Exclusion limits on the DM annihilation cross-section versus the particle mass are given in Section 5. Several DM particle candidates are considered, with particular emphasis on possible particle physics and astrophysical enhancements to the γ-ray annihilation flux.

2. Target selection and dark matter content

The Fornax (distance = 19 Mpc, Tonry *et al.* 2001), Coma (distance = 99 Mpc, Reiprich and Böhringer 2002) and Virgo (distance = 17 Mpc, Mei *et al.* 2007) galaxy clusters are in principle promising targets for indirect dark matter searches through γ-rays, as was shown by Jeltema *et al.* (2009). The radio galaxy M 87 at the center of Virgo provides a strong astrophysical γ-ray

signal (Aharonian *et al.* 2006a), showing flux variabilities from daily to yearly timescales that exclude the bulk of the signal to be of a DM origin. Since a DM γ-ray signal would be hard to disentangle from this dominant standard astrophysical signal, Virgo is not a prime target for DM searches, even though a DM signal may be hidden by the dominant γ-ray signal from standard astrophysical sources.

Moreover, galaxy clusters are expected to harbor a significant population of relativistic cosmic-ray protons originating from different sources, such as large-scale shocks associated with accretion and merger processes (Colafrancesco and Blasi 1998; Ryu *et al.* 2003), or supernovae (Völk *et al.* 1996) and AGN activity (Hinton *et al.* 2007). The γ-ray emission arising from pion decays produced by the interaction of these cosmic-ray protons with the intracluster gas may be a potential astrophysical background to the DM-induced γ-ray signal. In the case of Coma, Jeltema *et al.* (2009) showed that such astrophysical background is expected to be higher than the DM annihilation signal[1]. On the other hand, the same study ranked Fornax as the most luminous cluster in DM-induced γ-ray emission among a sample of 106 clusters from the HIFLUGCS catalog (Reiprich and Böhringer 2002). The DM-to-cosmic-ray γ-ray flux ratio of Fornax was predicted to be larger than 100 in the GeV energy range (Jeltema *et al.* 2009). A recent independent study by Pinzke *et al.* (2011) has also predicted Fornax to be among the brightest DM galaxy clusters with a favorably-low cosmic-ray induced signal. Although the central galaxy of the Fornax cluster, NGC 1399, is a radio galaxy and could in principle emit γ-rays , the super-massive black hole at the center of this galaxy have been shown to be passive (Pedaletti *et al.* 2011). Indeed recent observations of several clusters with the *Fermi*-LAT detector have shown no γ-ray signal (Ackermann *et al.* 2010b), and the most stringent limits on dark matter annihilation were derived from the Fornax observations (Ackermann *et al.* 2010a).

The center of Fornax galaxy cluster is located at RA(J2000.0) = $03^{\rm h}38^{\rm m}29\overset{\rm s}{.}3$ and Dec(J2000.0) = $-35^\circ\ 27'\ 00\overset{''}{.}7$ in the Southern Hemisphere. For ground-based Cherenkov telescopes like H.E.S.S. (cf. Section 3), low zenith angle observations are required to guarantee the lowest possible energy threshold and the maximum sensitivity of the instrument. Given the location of H.E.S.S., this condition is best fulfilled for Fornax, compared to the Virgo and Coma clusters. Therefore, Fornax is the preferred galaxy cluster target for dark matter searches for the H.E.S.S. experiment. The properties of its dark matter halo are discussed in more details in the following section.

[1]Also the two brightest radio galaxies, NGC 4874 and NGC 4889, lying in the central region of Coma may be potential sources of a standard astrophysical γ-ray signal.

2.1. Dark matter in the Fornax galaxy cluster

The energy-differential γ-ray flux from dark matter annihilations is given by the following equation:

$$\frac{\mathrm{d}\Phi_\gamma(\Delta\Omega, E_\gamma)}{\mathrm{d}E_\gamma} = \frac{1}{8\pi}\frac{\langle\sigma v\rangle}{m^2_{\mathrm{DM}}}\frac{\mathrm{d}N_\gamma}{\mathrm{d}E_\gamma} \times \overline{J}(\Delta\Omega)\Delta\Omega\,, \tag{1}$$

where $\langle\sigma v\rangle$ is the velocity-weighted annihilation cross-section, m_{DM} the mass of the DM particle and $\mathrm{d}N_\gamma/\mathrm{d}E_\gamma$ the photon spectrum per annihilation. The factor

$$\overline{J}(\Delta\Omega) = \frac{1}{\Delta\Omega}\int_{\Delta\Omega}\mathrm{d}\Omega\int_{\mathrm{LOS}}\mathrm{d}l \times \rho^2[r(l)] \tag{2}$$

reflects the dark matter density distribution inside the observing angle $\Delta\Omega$. The annihilation luminosity scales with the squared dark matter density ρ^2, which is conveniently parametrized as a function of the radial distance r from the center of the astrophysical object under consideration. This luminosity is integrated along the line of sight (LOS) and within an angular region $\Delta\Omega$, whose optimal value depends on the dark matter profile of the target and the angular resolution of the instrument.

Numerical simulations of structure formation in the ΛCDM framework predict cuspy dark matter halos in galaxies and clusters of galaxies (Navarro *et al.* 1996; Fukushige and Makino 1997; Moore *et al.* 1998). A prominent parametrization of such halos is the "Navarro-Frenk-White" (NFW) profile (Navarro *et al.* 1997), characterizing halos by their scale radius r_s at which the logarithmic slope is $\mathrm{d}\ln\rho/\mathrm{d}\ln r = -2$, and a characteristic density $\rho_s = 4\,\rho(r_s)$. This profile was shown to be consistent with X-ray observations of the intracluster medium of galaxy clusters. The DM density profile is given by:

$$\rho_{\mathrm{NFW}}(r) = \frac{\rho_s}{\left(\frac{r}{r_s}\right)\left(1+\frac{r}{r_s}\right)^2} \quad . \tag{3}$$

Another prediction of ΛCDM N-body simulations is an abundance of halo substructures, as will be detailed in section 2.2. On the other hand, in scenarios where the baryon infall in the DM gravitational potential efficiently transfers energy to the inner part of the DM halo by dynamical friction, a flattening of the density cusp into a core-halo structure is predicted (see e.g. El-Zant *et al.* 2001). These halos can be parametrized by the "Burkert profile" (Burkert 1996):

$$\rho_B(r) = \frac{\rho_0 r_c^3}{(r+r_c)(r^2+r_c^2)} \quad . \tag{4}$$

Again, the dark matter density falls off as $\sim r^{-3}$ outside the core radius r_c, but it approaches a constant value ρ_0 for $r \to 0$. In the following, dark matter halos of both types are considered.

A commonly-used approach for the determination of the DM halo in galaxy cluster comes from X-ray measurements of the gravitationally bound hot intracluster gas. From the HIFLUGCS catalog (Reiprich and Böhringer 2002), the virial mass and radius of Fornax are found to be $M_{\rm vir} \sim 10^{14}$ $M_\odot$ and $R_{\rm vir} \sim 1$ Mpc (corresponding to about 6° in angular diameter), respectively. Under the assumption of a NFW halo profile in ΛCDM cosmology, a relation between the virial mass and the concentration parameter $c = R_{\rm vir}/r_s$ was found by Buote *et al.* (2007). The halo parameters can thus be expressed in terms of ρ_s and r_s and are presented in Table 1. This model is hereafter referred as to RB02. A similar procedure was applied in the *Fermi*-LAT DM analysis of galaxy clusters (Ackermann *et al.* 2010a).

A different approach is to use dynamical tracers of the gravitational potential of the cluster halo, such as stars, globular clusters or planetary nebulae. This method is limited by the observability of such tracers, but can yield less model-dependent and more robust modeling of the DM distribution. However, some uncertainty is introduced by the translation of the tracer's velocity dispersion measurement into a mass profile, which usually implies solving the Jeans equations under some simplifying assumptions (Binney and Tremaine 2008). From velocity dispersion measurements on dwarf galaxies observed up to about 1.4 Mpc, a dynamical analysis of the Fornax cluster by Drinkwater *et al.* (2001) constrained the cluster mass. The associated DM density profile, hereafter referred as to DW01, can be well described by a NFW profile (Richtler *et al.* 2008) with parameters given in Table 1.

Richtler *et al.* (2008) have analyzed the DM distribution in the inner regions of Fornax by using the globular clusters as dynamical tracers. This allowed an accurate DM mass profile measurement out to a radial distance of 80 kpc from the galactic cluster centre, corresponding to an angular distance of $\sim 0.25^\circ$. The resulting velocity dispersion measurements can be well fitted by a NFW DM halo profile with parameters given in Table 1. This density profile (hereafter referred as to RS08) determination is in good agreement with the determination inferred from ROSAT-HRI X-ray measurements (Paolillo *et al.* 2002). Detailed analysis using subpopulations of globular clusters done in Schuberth *et al.* (2010) showed that both a NFW and a Burkert DM halo profiles can equally well fit the globular cluster velocity dispersion measurements. Representative DM halo profiles using different sets of globular clusters samples, hereafter referred as to SR10 a_6 and SR10 a_{10}, are extracted from Table 6 of Schuberth *et al.* (2010). The parameters for both the NFW and

Burkert DM halo profiles are given in Table 1.

Using the dark matter halo parameters derived from the above-mentioned methods, values of $\overline{J}$ were derived for different angular integration radii. The point-spread-function of H.E.S.S. corresponds to an integration angle of $\sim 0.1^\circ$ (Aharonian *et al.* 2006b), and most often the smallest possible angle is used in the search for dark matter signals in order to suppress background events. However, since a sizable contribution to the γ-ray flux may also arise from dark matter subhalos located at larger radii (see Section 2.2), integration angles of 0.5° and 1.0° were also considered. The choice of the tracer samples induces a spread in the values of the astrophysical factor $\overline{J}$ up to one order of magnitude for an integration angle of 0.1°. Note that the measurements of Richtler *et al.* (2008) and Schuberth *et al.* (2010) trace the DM density distribution only up to 80 kpc from the center. In consequence the derived values of the virial mass and radius are significantly smaller than those derived from X-ray measurements on larger distance scales (see for instance figure 22 of Schuberth *et al.* 2010). Thus the DM density values may be underestimated for distances larger than about 100 kpc. On the other hand, it is well known that for an NFW profile about 90% of the DM annihilation signal comes from the volume within the scale radius r_s. Therefore, even for NFW models with large virial radii such as RB02 and DW01, the main contribution to the annihilation signal comes from the region inside about 98 kpc and 220 kpc, respectively.

2.2. Dark matter halo substructures

Recent cosmological N-body simulations, such as Aquarius (Springel *et al.* 2008) and Via Lactea (Diemand *et al.* 2008), have suggested the presence of dark matter substructures in the form of self-bound overdensities within the main halo of galaxies. A quantification of the substructure flux contribution to the total γ-ray flux was computed from the Aquarius simulation by Pinzke *et al.* (2009) using the NFW profile RB02 as the DM density distribution of the smooth halo[2]. The substructure enhancement over the smooth host halo contribution along the line of sight is defined as $B_\mathrm{sub}(\Delta\Omega) = 1 + \mathcal{L}_\mathrm{sub}(\Delta\Omega)/\mathcal{L}_\mathrm{sm}(\Delta\Omega)$, where $\mathcal{L}_\mathrm{sm/sub}(\Delta\Omega)$ denotes the annihilation luminosity of the smooth host halo and the

[2]This halo is also well suited with respect to the others discussed in Section2.1 since substructures in the form of gravitationally bound dwarf galaxies to Fornax are observed up to about 1 Mpc. They are thus included within the virial radius predicted by the RB02 profile ($R_\mathrm{vir} \simeq 1$ Mpc).

			$\overline{J}(\Delta\Omega)$ [10^{21} GeV^{2}cm^{-5}]		
			NFW profile		
Model	r_s [kpc]	ρ_s [$M_\odot pc^{-3}$]	$\theta_{max} = 0.1°$	$\theta_{max} = 0.5°$	$\theta_{max} = 1.0°$
RB02	98	0.0058	112.0	6.5	1.7
DW01	220	0.0005	6.2	0.5	0.1
RS08	50	0.0065	24.0	1.2	0.3
SR10 a_{10}	34	0.0088	15.0	0.6	0.1
SR10 a_6	200	0.00061	7.0	0.5	0.1
			Burkert profile		
Model	r_c [kpc]	ρ_c [$M_\odot pc^{-3}$]	$\theta_{max} = 0.1°$	$\theta_{max} = 0.5°$	$\theta_{max} = 1.0°$
SR10 a_{10}	12	0.0728	15.0	0.6	0.2
SR10 a_6	94	0.0031	2.4	0.5	0.1

Table 1: Dark matter halo models for the Fornax galaxy cluster. The first three columns show the selected profiles discussed in Section 2.1 with their respective NFW or Burkert halo parameters. The last three columns show the astrophysical factor $\overline{J}$, calculated for three different integration radii.

additional contribution from substructures, respectively. The former is defined by:

$$\mathcal{L}_{\rm sm/sub}(\Delta\Omega) \;=\; \Delta\Omega \times \overline{J}_{\rm sm/sub}(\Delta\Omega) \;=\; \int_{\Delta\Omega} {\rm d}\Omega \int_{\rm l.o.s.} {\rm d}l \times \rho^2_{\rm sm/sub}[r(l)]\,, \tag{5}$$

where $\rho_{\rm sm/sub}$ is the DM density distribution of the smooth halo and substructures, respectively. In order to perform the LOS integration over the subhalo contribution, an effective substructure density $\tilde{\rho}_{\rm sub}$ is parametrized following Springel *et al.* (2008) and Pinzke *et al.* (2009) as:

$$\tilde{\rho}^2_{\rm sub}(r) = \frac{A(r)\,0.8C\,\mathcal{L}_{\rm sm}(R_{\rm vir})}{4\pi r^2 R_{\rm vir}} \left(\frac{r}{R_{\rm vir}}\right)^{-B(r)}\,, \tag{6}$$

where

$$A(r) = 0.8 - 0.252\ln(r/R_{\rm vir}) \tag{7}$$

and

$$B(r) = 1.315 - 0.8(r/R_{\rm vir})^{-0.315}\,. \tag{8}$$

$\mathcal{L}_{\rm sm}({\rm R_{vir}})$ is the smooth halo luminosity within the virial radius $R_{\rm vir}$. The normalization is given by $C = (M_{\rm min}/M_{\rm lim})^{0.226}$, where $M_{\rm min} = 10^5 M_\odot$ is the minimum substructure mass resolved in the simulation and $M_{\rm lim}$ is the intrinsic limiting mass of substructures, or free-streaming mass. A conventional value for this quantity is $M_{\rm lim} =$

$10^{-6}M_\odot$ (Diemand *et al.* 2006), although a rather broad range of values, down to $M_{\rm lim} = 10^{-12}M_\odot$, is possible for different models of particle dark matter (Bringmann 2009). Assuming a specific DM model, a constraint on $M_{\rm lim}$ was derived by Pinzke *et al.* (2009) using EGRET γ-ray upper limits on the Virgo cluster and a lower bound was placed at $M_{\rm lim} = 5 \times 10^{-3}M_\odot$. Nevertheless, the effect of a smaller limiting mass is also investigated in this work.

Figure 1 shows the substructure enhancement $B_{\rm sub}$ over the smooth halo as function of the opening integration angle. At the distance of Fornax, integration regions larger than $\sim 0.2^\circ$ correspond to more than 65 kpc. Beyond these distances the substructure enhancement exceeds a factor 10. This justifies *extended* analyses using integration angles of 0.5° and 1.0°. Two values of the limiting mass of substructures are used: $M_{\rm lim} = 10^{-6}M_\odot$ and $M_{\rm lim} = 5 \times 10^{-3}M_\odot$, inducing a *high* and a *medium* value of the enhancement, respectively. The values of $B_{\rm sub}$ for the opening angles of 0.1°, 0.5° and 1.0° and for both values of $M_{\rm lim}$ are given in Table 2. These values are larger than those derived in Ackermann *et al.* (2010a). In their study the substructure enhancement is calculated from the Via Lactea (Diemand *et al.* 2008) simulation, where a different concentration mass relation is obtained. For a careful comparison see Pieri *et al.* (2011).

$\theta_{\rm max}$	0.1°	0.5°	1.0°
$M_{\rm lim} = 10^{-6}M_\odot$	4.5	50.5	120
$M_{\rm lim} = 5 \times 10^{-3}M_\odot$	1.5	8.2	18.3

Table 2: Enhancement $B_{\rm sub}$ due to the halo substructure contribution to the DM flux, for different opening angles of integration $\theta_{\rm max}$. The enhancement is calculated for two limiting masses of substructures $M_{\rm lim}$ and over the smooth DM halo RB02.

3. Observations and data analysis

The High Energy Stereoscopic System (H.E.S.S.) consists of four identical imaging atmospheric Cherenkov telescopes. They are located in the Khomas Highland of Namibia ($23^\circ16'18''$ South, $16^\circ30'00''$ East) at an altitude of 1800 m above sea level. The H.E.S.S. array was designed to observe VHE γ-rays through the Cherenkov light emitted by charged particles in the electromagnetic showers initiated by these γ-rays when entering the atmosphere. Each telescope has an optical reflector consisting of 382 round facets of 60 cm diameter each, yielding a total mirror area of 107 m^2 (Bernlöhr *et al.* 2003). The Cherenkov light is focused on cameras equipped with 960 photomultiplier tubes, each one subtending a field of view of 0.16°. The total field of view is $\sim 5^\circ$ in diameter. A stereoscopic

reconstruction of the shower is applied to retrieve the direction and the energy of the primary γ-ray.

Dedicated observations of the Fornax cluster, centered on NGC 1399, were conducted in fall 2005 (Pedaletti *et al.* 2008). They were carried out in *wobble mode* (Aharonian *et al.* 2006b), *i.e.* with the target typically offset by 0.7° from the pointing direction, allowing simultaneous background estimation from the same field of view. The total data passing the standard H.E.S.S. data-quality selection (Aharonian *et al.* 2006b) yield an exposure of 14.5 hrs live time with a mean zenith angle of 21°.

The data analysis was performed using an improved *model* analysis as described in de Naurois and Rolland (2009), with independent cross-checks performed with the *Hillas*-type analysis procedure (Aharonian *et al.* 2006b). Both analyses give compatible results. Three different signal integration angles were used, 0.1°, 0.5° and 1°. The cosmic-ray background was estimated with the *template* model (Rowell 2003), employing the source region, but selecting only hadron-like events from image cut parameters.

No significant excess was found above the background level in any of the integration regions, as visible in Fig. 2 for an integration angle of 0.1°. An upper limit on the total number of observed γ-rays, $N_\gamma^{95\%\,\mathrm{C.L.}}$, was calculated at 95% confidence level (C.L.). The calculation followed the method described in Feldman and Cousins (1998), using the number of γ-ray candidate events in the signal region N_{ON} and the *normalized* number of γ-ray events in the background region $\overline{N}_{\mathrm{OFF}}$. Since the normalization is performed with respect to the direction-dependent acceptance and event rate, the background normalization factor for $\overline{N}_{\mathrm{OFF}}$ as defined in Rowell (2003) is $\alpha \equiv 1$. This is equivalent to the assumption that the uncertainty on the background determination is the same as for the signal, allowing a conservative estimate of the upper limits. This information is summarized in Table 3.

A minimal γ-ray energy (E_{min}) is defined as the energy at which the acceptance for point-like observations reaches 20% of its maximum value, which gives 260 GeV for the observations of Fornax. Limits on the number of γ-ray events above the minimal energy E_{min} have also been computed (see Table 4) and are used in Section 4 for the calculation of upper limits on the γ-ray flux.

4. γ-ray flux upper limits

Upper limits on the number of observed γ-rays above a minimal energy E_{min} can be translated into an upper limit on the observed γ-ray flux Φ_γ if the energy spectrum

$\theta_{\rm max}$	$\rm N_{ON}$	$\overline{\rm N}_{\rm OFF}$	$N_\gamma^{95\%\,\rm C.L.}$	Significance
0.1°	160	122	71	2.3
0.5°	3062	2971	243	1.2
1.0°	11677	11588	388	0.6

Table 3: Numbers of VHE γ-ray events from the direction of the Fornax galaxy cluster centre, using three different opening angles for the observation. Column 1 gives the opening angle $\theta_{\rm max}$, columns 2 and 3 the numbers of γ-ray candidates in the ON region, $\rm N_{ON}$, and the normalized number of γ-ray in the OFF region, $\overline{\rm N}_{\rm OFF}$, respectively. Column 4 gives the 95% C.L. upper limit on the number of γ-ray events according to Feldman and Cousins (1998). The significance of the numbers of γ-ray candidates in the ON region is stated in column 5 according to Li and Ma (1983).

$\mathrm{d}N_\gamma/\mathrm{d}E_\gamma$ of the source is assumed to be known, as indicated by equation 9.

$$\Phi_\gamma^{95\%\,\rm C.L.}(E_\gamma > E_{\rm min}) = \frac{N_\gamma^{95\%\,\rm C.L.}(E_\gamma > E_{\rm min}) \int_{E_{\rm min}}^{\infty} \mathrm{d}E_\gamma \frac{\mathrm{d}N_\gamma}{\mathrm{d}E_\gamma}(E_\gamma)}{T_{\rm obs} \int_{E_{\rm min}}^{\infty} \mathrm{d}E_\gamma\, A_{\rm eff}(E_\gamma) \frac{\mathrm{d}N_\gamma}{\mathrm{d}E_\gamma}(E_\gamma)}\,. \tag{9}$$

Here, $T_{\rm obs}$ and $A_{\rm eff}$ denote the target observation time and the instrument's effective collection area, respectively. The intrinsic spectra of standard astrophysical VHE γ-ray sources (Hinton and Hofmann 2009) typically follow power-law behavior of index $\Gamma \approx 2-3$. Upper limits at 95% C.L. on the integral flux above the minimum energy (cf. Section 3) are given in Table 4 for different source spectrum indices.

Dark matter annihilation spectra depends on the assumed annihilation final states of the DM model. For instance, some supersymmetric extensions of the Standard Model (Jungman *et al.* 1996) predict the *neutralino* as the lightest stable supersymetric particle, which would be a good dark matter candidate. In general, the self-annihilation of neutralinos will give rise to a continuous γ-ray spectrum from the decay of neutral pions, which are produced in the hadronisation process of final-state quarks and gauge bosons. Universal extra-dimensional (UED) extensions of the SM also provide suitable DM candidates. In these models, the first Kaluza-Klein (KK) mode of the hypercharge gauge boson $\widetilde{B}^{(1)}$ is the lightest KK particle (LKP) and it can be a DM particle candidate (Servant and Tait 2003). Nevertheless, in the absence of a preferred DM particle model, constraints are presented here in a model-independent way, i.e. for given pure pair annihilation final state for the DM pair annihilation processes and DM particle mass. The only specific DM particle model studied here is the KK $\widetilde{B}^{(1)}$ particle model, where the branching ra-

tios of each annihilation channel are known. A wide range of dark matter masses is investigated from about 100 GeV up to 100 TeV. A model-independent upper bound on the dark matter mass can be derived from unitarity for thermally produced DM as done in the seminal paper of Griest and Kamionkowski (1990) and subsequent studies of Beacom *et al.* (2007) and Mack *et al.* (2008). Assuming the current DM relic density measured by WMAP (Larson *et al.* 2011), the inferred value is about 100 TeV. Figure 3 shows different annihilation spectra for 1 TeV mass dark matter particles. Spectra of DM particles annihilating into $b\bar{b}$, W^+W^- and $\tau^+\tau^-$ pairs are extracted from Cirelli *et al.* (2011), and calculated from Servant and Tait (2003) for Kaluza-Klein $\widetilde{B}^{(1)}$ annihilation. Flux upper limits as function of the DM particle mass are presented in Figure 4 assuming DM annihilation purely into $b\bar{b}$, W^+W^- and $\tau^+\tau^-$ and an opening angle of the integration of 0.1°. Flux upper limits reaches 10^{-12} cm^{-2} s^{-1} for 1 TeV DM mass.

$\theta_{\rm max}$	$N_\gamma^{95\%\,\rm C.L.}(E_\gamma > E_{\rm min})$	$\Phi_\gamma^{95\%\,\rm C.L.}(E_\gamma > E_{\rm min})(10^{-12}$ cm^{-2} s$^{-1})$	
		$\Gamma = 1.5$	$\Gamma = 2.5$
0.1°	41.3	0.8	1.0
0.5°	135.1	2.3	3.3
1.0°	403.5	6.8	10.0

Table 4: Upper limits on the VHE γ-ray flux from the direction of Fornax, assuming a power-law spectrum with spectral index Γ between 1.5 and 2.5. Column 1 gives the opening angle of the integration region $\theta_{\rm max}$, column 2 the upper limits on the number of observed γ-rays above the minimum energy $E_{\rm min} = 260$ GeV, calculated at 95% C.L.. Columns 3 and 4 list the 95% C.L. integrated flux limits above the minimum energy, for two power law indices.

Recent studies (Jeltema *et al.* 2009; Pinzke *et al.* 2009; Pinzke and Pfrommer 2010) have computed the cosmic-ray induced γ-ray flux from pion decays using a cosmological simulation of a sample of 14 galaxy clusters (Pfrommer *et al.* 2008). Since the electron induced γ-ray flux from inverse Compton is found to be systematically subdominant compared to the pion decay γ-ray flux (Jeltema *et al.* 2009), this contribution is not considered. Using the results of Pinzke *et al.* (2009), the γ-ray flux above 260 GeV for Fornax is expected to lie between a few 10^{-15} cm^{-2} s^{-1} and 10^{-14} cm^{-2} s^{-1} for an opening angle of observation of 1.0°. The flux is about 2-to-3 orders of magnitude lower than the upper limits presented in Table 4, thus this scenario cannot be constrained.

Assuming a typical value of the annihilation cross-section for thermally-produced DM, $\langle\sigma v\rangle = 3\times10^{-26}$ cm^{3}s^{-1}, a mass of 1 TeV and the NFW profile of DM density profile of Fornax RB02, the predicted DM γ-ray flux is found to be a few 10^{-13} cm^{-2} s^{-1}. This

estimate takes into account the γ-ray enhancement due to dark halo substructure and the Sommerfeld enhancement (see section 5) to the overall DM γ-ray flux. Therefore the dominant γ-ray signal is expected to originate from DM annihilations. Constraints on the DM-only scenario are derived in the following section.

5. Exclusion limits on dark matter annihilations

Upper limits at 95% C.L. on the dark matter velocity-weighted annihilation cross-section can be derived from the following formula:

$$\langle \sigma v \rangle^{95\%\,\mathrm{C.L.}} = \frac{8\pi}{T_{\mathrm{obs}}} \frac{m_{\mathrm{DM}}^2}{\overline{J}(\Delta\Omega)\Delta\Omega} \frac{N_\gamma^{95\%\,\mathrm{C.L.}}}{\int_0^{m_{\mathrm{DM}}} \mathrm{d}E_\gamma \, A_{\mathrm{eff}}(E_\gamma) \dfrac{\mathrm{d}N_\gamma(E_\gamma)}{\mathrm{d}E_\gamma}} \,. \tag{10}$$

The factor $\overline{J}$ is extracted from Section 2. The exclusion limits as a function of the DM particle mass m_{DM} for different DM halo profile models are depicted in Figures 5 and 6 for DM particles annihilating exclusively into $b\overline{b}$ and $\widetilde{B}^{(1)}$ particles, respectively. Predictions for $\langle \sigma v \rangle$ as function of the $\widetilde{B}^{(1)}$ particle mass are given in Figure 6 within the UED framework of Servant and Tait (2003). As an illustration of a possible change in this prediction, a range of predicted $\langle \sigma v \rangle$ is extracted from Figure 2 of Arrenberg *et al.* (2008), in the case of a mass splitting between the LKP and the next lightest KK particle down to 1%. In the TeV range the 95% C.L. upper limit on the annihilation cross-section $\langle \sigma v \rangle$ reaches 10^{-22} cm^{3}s^{-1}. Exclusion limits as a function of the DM particle mass m_{DM} assuming DM particle annihilating into $b\overline{b}$, $\tau^+\tau^-$ and W^+W^- are presented in Figure 7 for the RB02 NFW profile. Stronger constraints are obtained for masses below 1 TeV in the $\tau^+\tau^-$ where the 95% C.L. upper limit on $\langle \sigma v \rangle$ reaches 10^{-23} cm^{3}s^{-1}. The *Fermi*-LAT exclusion limit for Fornax is added in Figure 5 (pink dashed-line), extending up to 1 TeV (Ackermann *et al.* 2010a). It is based on the RB02 NFW profile and a γ-ray spectrum which assumes annihilation to $b\overline{b}$ pairs. Below 1 TeV, the *Fermi*-LAT results provide stronger limits than the H.E.S.S. results. However, the H.E.S.S. limits well complement the DM constraints in the TeV range.

Other DM particle models give rise to modifications of the γ-ray annihilation spectrum which may increase the predicted γ-ray flux. Some of them are considered in the following.

5.1. Radiative correction: Internal bremsstrahlung

In the annihilation of dark matter particles to charged final states, internal bremsstrahlung processes can contribute significantly to the high-energy end of the γ-ray spectrum (Bergström *et al.* 2005; Bringmann *et al.* 2008). Adding this effect to the continuous spectrum of secondary γ-rays from pion decay, the total spectrum is given by

$$\frac{dN_\gamma}{dE_\gamma} = \frac{dN_\gamma^{\rm sec}}{dE_\gamma} + \frac{dN_\gamma^{\rm IB}}{dE_\gamma} \, . \tag{11}$$

The magnitude of this effect depends on the intrinsic properties of the dark matter particle. Bringmann *et al.* (2008) provide an approximation that is valid for wino-like neutralinos (Moroi and Randall 2000). The annihilation spectrum for a 1 TeV wino is shown in Figure 3. This parametrization is used in the calculation of the 95% C.L. upper limit on the velocity-weighted annihilation cross-section as a function of the DM particle mass, presented in Figures 7 and 8. The internal bremsstrahlung affects the exclusion limits mostly in the low mass DM particle regime, where its contribution to the total number of γ-rays in the H.E.S.S. acceptance is largest.

5.2. *Leptophilic* models

Recent measurements of cosmic electron and positron spectra by PAMELA (Adriani *et al.* 2009), ATIC (Chang *et al.* 2008), H.E.S.S. (Aharonian *et al.* 2009b) and *Fermi*-LAT (Ackermann *et al.* 2010c) have been explained in terms of DM annihilation primarily into leptonic final states (to avoid an over-production of anti-protons), hereafter referred to as *leptophilic* models. Bergström *et al.* (2009) show that the *Fermi*-LAT electron spectrum and the PAMELA excess in positron data can be well explained by annihilation purely into $\mu^+\mu^-$ pairs. In this scenario, γ-rays are expected from final state radiation (FSR) of the $\mu^+\mu^-$ pair. While this final state is rarely found in supersymmetric models (Jungman *et al.* 1996), some particle physics models predict the annihilation to occur predominantly to lepton final states (Arkani-Hamed *et al.* 2009; Nomura and Thaler 2009). The subsequent muon decay into positrons and electrons may lead to an additional γ-ray emission component by Inverse Compton (IC) up-scattering of background photons, such as those of the cosmic microwave background (CMB). If the electron/positron energy loss time scale is much shorter than the spatial diffusion time scale, the IC contribution to the γ-ray flux may be significant. In galaxy clusters, the energy loss term is dominated by the IC compo-

nent (Colafrancesco *et al.* 2006). The total γ-ray spectrum is then given by

$$\frac{dN_\gamma}{dE_\gamma} = \frac{dN_\gamma^{\rm FSR}}{dE_\gamma} + \frac{dN_\gamma^{\rm IC}}{dE_\gamma} \, . \tag{12}$$

After extracting the FSR parametrization from Bovy (2009), the IC component of the annihilation spectrum was calculated following the method described in Profumo and Jeltema (2009). The total annihilation spectrum for a 1 TeV dark matter particle annihilating to $\mu^+\mu^-$ pairs is shown in Figure 3. The energy $\mathrm{E}_\gamma^{\rm IC}$ of the IC emission peak is driven by electrons/positrons of energy $\mathrm{E_e} \sim m_{\rm DM}/2$ up-scattering target photons in a radiation field of average energy $\epsilon = 2.73$ K and is given by $E_\gamma^{\rm IC} \approx \epsilon(E_{\rm e}/m_{\rm e})^2$ (Longair 1992). Consequently, the enhancement of the γ-ray flux in the H.E.S.S. energy range is found to lower the exclusion limits only for very high DM masses, $m_{\rm DM} > 10$ TeV. The limits are enhanced by a factor of $\sim$10. The *Fermi*-LAT exclusion limit for Fornax is added (gray dashed-line), extending up to 10 TeV (Ackermann *et al.* 2010a). Due to the IC component, below a few tens of TeV the *Fermi*-LAT results provide stronger limits than the H.E.S.S. results. However, since for DM particle masses above 10 TeV the IC emission peak falls out of the *Fermi*-LAT energy acceptance, the IC spectra becomes harder in the same energy range. The *Fermi*-LAT limits for DM particle masses above 10 TeV would tend to raise with a stronger slope than the slope in between 1 and 10 TeV. Thus H.E.S.S. limits would well-complement the *Fermi*-LAT constraints in the DM mass range higher than 10 TeV.

γ-rays from IC emission are also expected in the case of DM particles annihilating purely into $b\overline{b}$. In the H.E.S.S. energy range for high DM masses ($\gtrsim$ 10 TeV) annihilating in the $b\overline{b}$ channel, the expected number of γ-rays including IC emission is lower than in the $\mu^+\mu^-$ channel (see, for instance, Cirelli *et al.* 2011). This qualitative estimate in the *Fermi*-LAT energy range (80 MeV - 300 GeV) shows that the number of expected γ-rays including IC emission for DM particle masses between 1 and 10 TeV is lower in the $b\overline{b}$ than in the $\mu^+\mu^-$ channel by at least a factor of 2. Since the $\langle\sigma v\rangle$ exclusion limits are roughly scaled by the number of expected γ-rays , a qualitative estimate of the *Fermi*-LAT limits including the IC component in the $b\overline{b}$ channel should not be better than their limits in the $\mu^+\mu^-$ channel.

5.3. *Sommerfeld* enhancement

The self-annihilation cross-section of dark matter particles can be enhanced with respect to its value $\langle\sigma v\rangle_0$ during thermal freeze-out by the *Sommerfeld effect* (see e.g. Hisano *et al.* 2004; Profumo 2005). This is a velocity-dependent quantum mechanical effect: If the relative velocity of two annihilating particles is sufficiently low, the effective annihilation

cross-section can be boosted by multiple exchange of the force carrier bosons. This can be parametrized by a boost factor S, as defined by:

$$\langle \sigma v \rangle_{\rm eff} = S \times \langle \sigma v \rangle_0 \,. \tag{13}$$

Lattanzi and Silk (2009) consider the case of a Sommerfeld boost due to the weak force which can arise if the dark matter particle is a wino-like neutralino. As a result of the masses and couplings of the weak gauge bosons, the boost is strongest for a DM particle mass of about 4.5 TeV, with resonance-like features appearing for higher masses. This effect was proposed to account for the PAMELA/ATIC data excess, where a boost of 10^4 or more is required for neutralinos with masses of 1–10 TeV (Cirelli *et al.* 2009). It was shown that the boost would be maximal in the dwarf galaxies and in their substructures (Pieri *et al.* 2009), due to the low DM particle velocity dispersion in these objects.

In the Fornax galaxy cluster, the velocity dispersion and hence the mean relative velocity of "test masses" such as stars, globular clusters or galaxies is of the order of a few 100 km s^{-1} (Schuberth *et al.* 2010), hence $\beta = \frac{<v_{\rm rel}>}{c} \approx 10^{-3}$. Assuming that the same velocity distribution holds true for DM particles, limits on $\langle \sigma v \rangle_{\rm eff}/S$ were derived which are shown in Figure 8 for a signal integration radius of 1.0° and the RB02 NFW profile. Although the DM velocity dispersion is about one order of magnitude higher than in dwarf galaxies, a boost of $\sim 10^3$ is obtained for DM particle masses around 4.5 TeV. The resonance-like feature is clearly visible for masses above 4.5 TeV. Outside the resonances, the limits on $\langle \sigma v \rangle_{\rm eff}/S$ are tightened by more than one order of magnitude for dark matter particles heavier than about 3 TeV.

5.4. Enhancement from dark matter substructures

The effect of DM substructures inside the opening angle of 0.1° and 1.0° are presented in Figure 9, using the enhancement values calculated in Section 2.2. The enhancements to the 95% C.L. upper limits on $\langle \sigma v \rangle$ are estimated using the two limiting masses of substructures $M_{\rm lim}$. In the TeV range, the upper limit on $\langle \sigma v \rangle$ is at the 10^{-23} cm^{3}s^{-1} level. The joint enhancement due to the Sommerfeld effect added to the IB and the substructures contribution is plotted in Figure 8. In the most optimistic model, with the largest enhancement by substructures and the Sommerfeld effect, the 95% C.L. upper limit on $\langle \sigma v \rangle_{\rm eff}$ reaches 10^{-26} cm^{3}s^{-1}, thus probing natural values for thermally-produced DM.

6. Summary

The Fornax galaxy cluster was observed with the H.E.S.S. telescope array to search for VHE γ-rays from dark matter self-annihilation. No significant γ-ray signal was found and upper limits on the γ-ray flux were derived for power-law and DM spectra, at the level of 10^{-12} cm^{-2}s^{-1} above 260 GeV .

Assuming several different models of particle dark matter and using published models of the dark matter density distribution in the halo, exclusion limits on the DM self-annihilation cross-section as a function of the DM particle mass were derived. Particular consideration was given to possible enhancements of the expected γ-ray flux which could be caused by DM halo substructure or the Sommerfeld effect. For a DM mass of 1 TeV, the exclusion limits reach values of $\langle\sigma v\rangle \approx 10^{-22} - 10^{-23}$ cm^{3}s^{-1}, depending on DM model and halo properties, without the substructures contribution, and $\langle\sigma v\rangle \approx 10^{-23} - 10^{-24}$ cm^{3}s^{-1} when considering the substructures signal enhancement. At $M_{\rm DM} \approx 4.5$ TeV, a possible Sommerfeld resonance could lower the upper limit to 10^{-26} cm^{3}s^{-1}.

Compared to observations of dwarf spheroidal galaxies (see for instance Abramowski *et al.* 2011a) or globular clusters (Abramowski *et al.* 2011b), these limits reach roughly the same order of magnitude. The choice of different tracers to derive the DM halo profile in Fornax galaxy cluster allows to well constraint the uncertainty in the expected signal. The poorly constrained, but plausibly stronger subhalo enhancement in the Fornax cluster induces a uncertainty in the expected signal of about two orders of magnitude.

With an optimistic joint γ-ray signal enhancement by halo substructures and the Sommerfeld effect, the limits on $\langle\sigma v\rangle$ reach the values predicted for thermal relic dark matter. Additionally, they extend the exclusions calculated from *Fermi*-LAT observations of galaxy clusters to higher DM particle masses.

The support of the Namibian authorities and of the University of Namibia in facilitating the construction and operation of H.E.S.S. is gratefully acknowledged, as is the support by the German Ministry for Education and Research (BMBF), the Max Planck Society, the French Ministry for Research, the CNRS-IN2P3 and the Astroparticle Interdisciplinary Programme of the CNRS, the U.K. Particle Physics and Astronomy Research Council (PPARC), the IPNP of the Charles University, the South African Department of Science and Technology and National Research Foundation, and by the University of Namibia. We appreciate the excellent work of the technical support staff in Berlin, Durham, Hamburg, Heidelberg, Palaiseau, Paris, Saclay, and in Namibia in the construction and operation of the equipment.

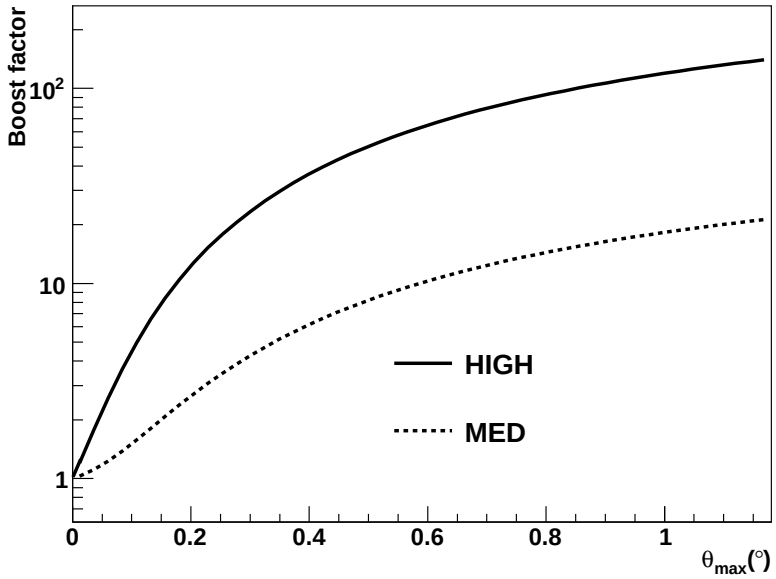

Fig. 1.— Substructure γ-ray flux enhancement as function of the opening angle of integration. Two values of the limiting mass of substructures are used: $M_{\rm lim} = 10^{-6} M_\odot$, for the high (HIGH) boost (solid line), and $M_{\rm lim} = 5 \times 10^{-3} M_\odot$, for the medium (MED) boost (dashed line). The RB02 profile is chosen as the smooth host DM halo.

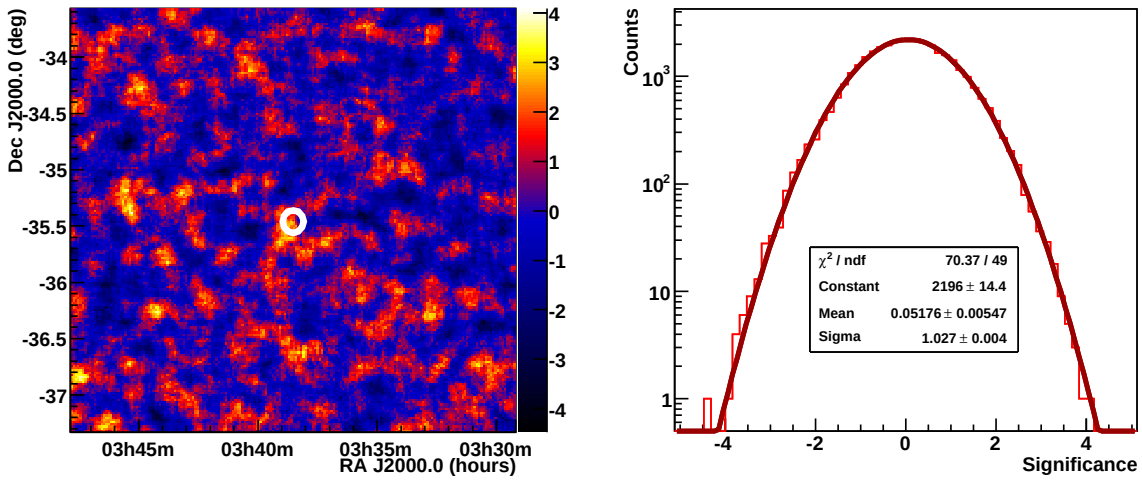

Fig. 2.— Left: Significance map in equatorial coordinates, calculated according to the Li & Ma method (Li and Ma 1983), with an oversampling radius of 0.1° . The white circle denotes the 0.1° integration region. No significant excess is seen at the target position. Right: Distribution of the significance. The solid line is a Gaussian fitted to the data. The significance distribution is well described by a normal distribution.

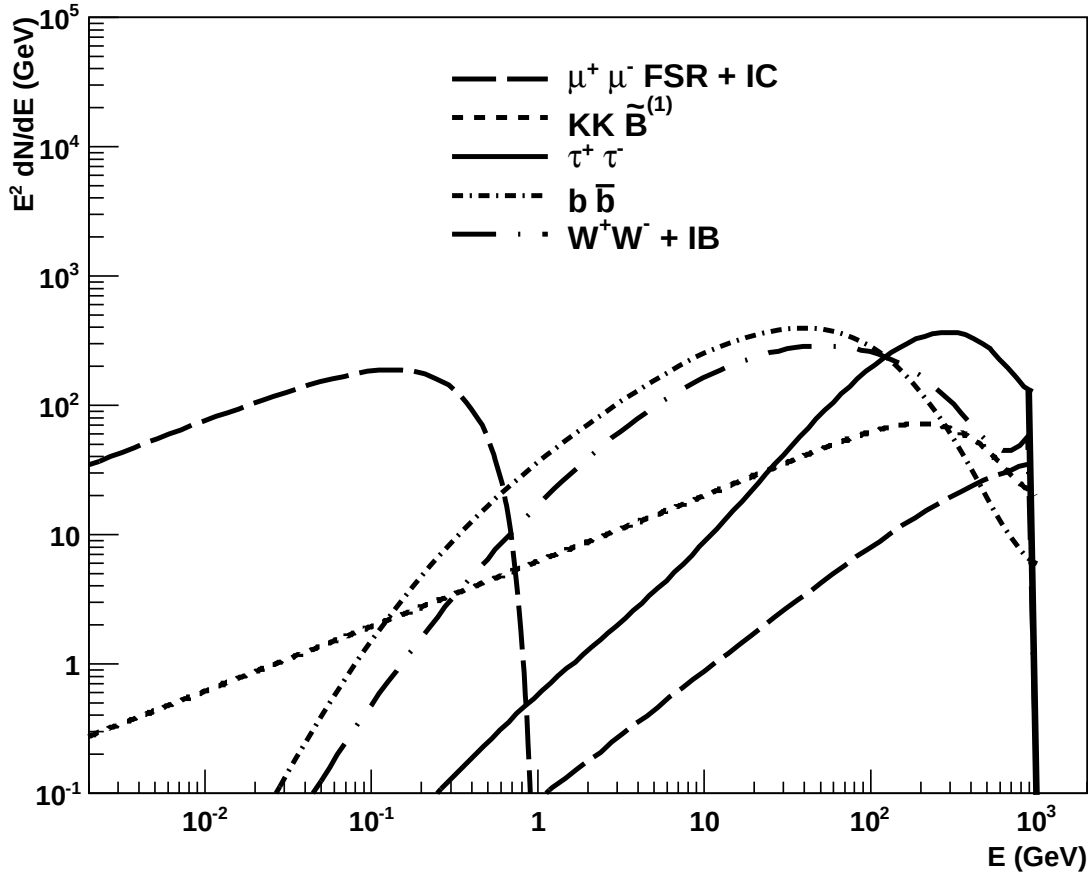

Fig. 3.— Photon spectra for 1 TeV dark matter particles self-annihilating in different channels. Spectra from DM annihilating purely into $b\overline{b}$ (dot-dashed line), $\tau^+\tau^-$ (black solid line) and W^+W^- (long-dashed dotted line) are shown. The latter shows the effect of Internal Bremsstrahlung (IB) occuring for the W^+W^- channel. The γ-ray spectrum from the annihilation of $\widetilde{B}^{(1)}$ hypergauge boson pairs arising in Kaluza-Klein (KK) models with UED is also plotted (dotted line). The long dashed line show the photon spectra from final-state radiation (FSR) and the inverse Compton (IC) scattering contribution in the case of DM particles annihilating into muon pairs.

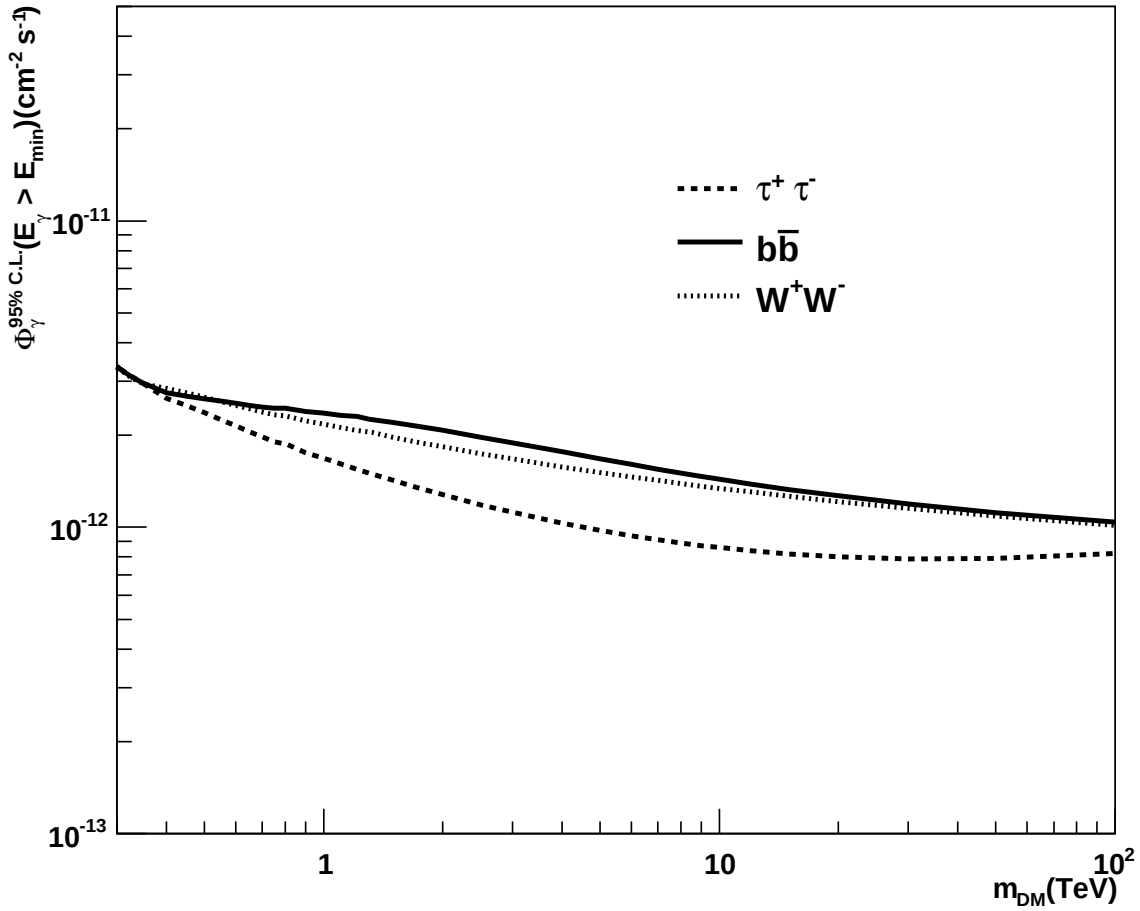

Fig. 4.— Upper limits 95% C.L. on the γ-ray flux as a function of the DM particle mass for E_{min}= 260 GeV from the direction of Fornax. DM particles annihilating into $b\bar{b}$ (solid line) , W^+W^- (dotted line) and $\tau^+\tau^-$ (dashed line) pairs are considered.

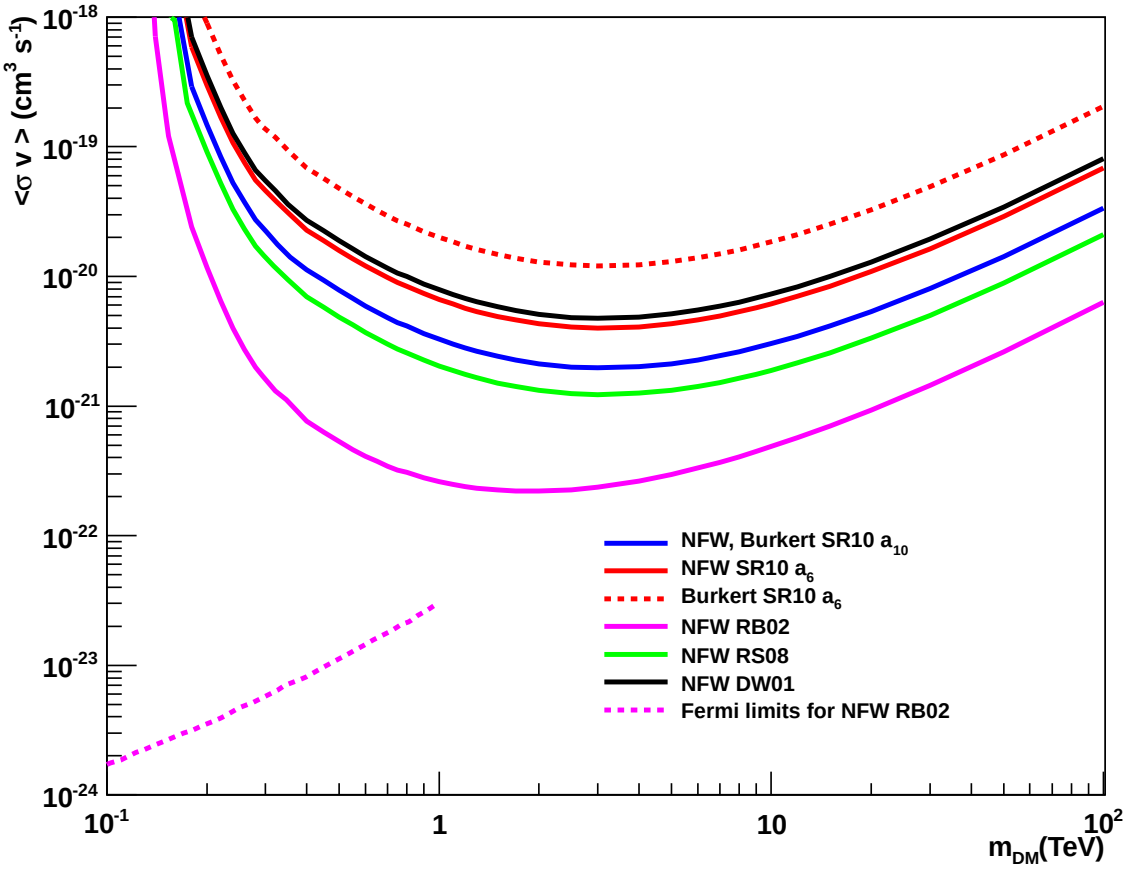

Fig. 5.— Upper limit at 95% C.L. on the velocity-weighted annihilation cross-section $\langle \sigma v \rangle$ as a function of the DM particle mass, considering DM particles annihilating purely into $b\bar{b}$ pairs. The limits are given for an integration angle $\theta_{\rm max} = 0.1^\circ$. Various DM halo profiles are considered: NFW profiles, SR10 a_{10} (blue solid line), DW01 (black solid line), RB02 (pink solid line) and RS08 (green solid line), and Burkert profiles, SR10 a_6 (red dotted line) and a_{10} (blue solid line). See Table 1 for more details. The *Fermi*-LAT upper limits (Ackermann *et al.* 2010a) for the NFW profile RB02 are also plotted.

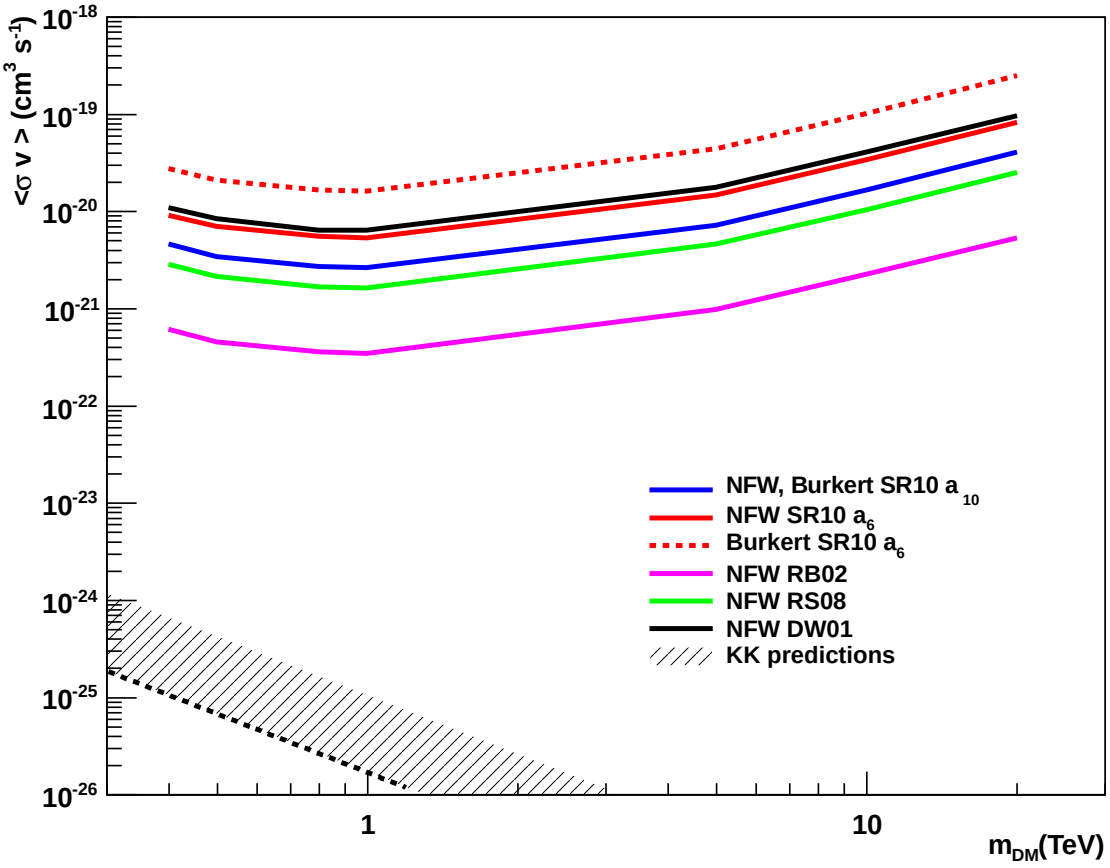

Fig. 6.— Kaluza-Klein hypergauge boson $\tilde{B}^{(1)}$ dark matter: Upper limit at 95% C.L. on $\langle\sigma v\rangle$ as function of the $\tilde{B}^{(1)}$ mass towards Fornax. The limits are given for an integration angle $\theta_{\rm max}$ = 0.1°. The NFW profiles, SR10 a_{10} (blue solid line), DW01 (black solid line), RB02 (pink solid line) and RS08 (green solid line), and Burkert profiles, SR10 a_6 (red dotted line) and a_{10} (blue solid line). See Table 1 for more details. The prediction of $\langle\sigma v\rangle$ as function of the $\tilde{B}^{(1)}$ mass is given (dotted-line). A range for this predictions is given in case of a mass splitting between the LKP and the next LKP down to 1% (dashed area).

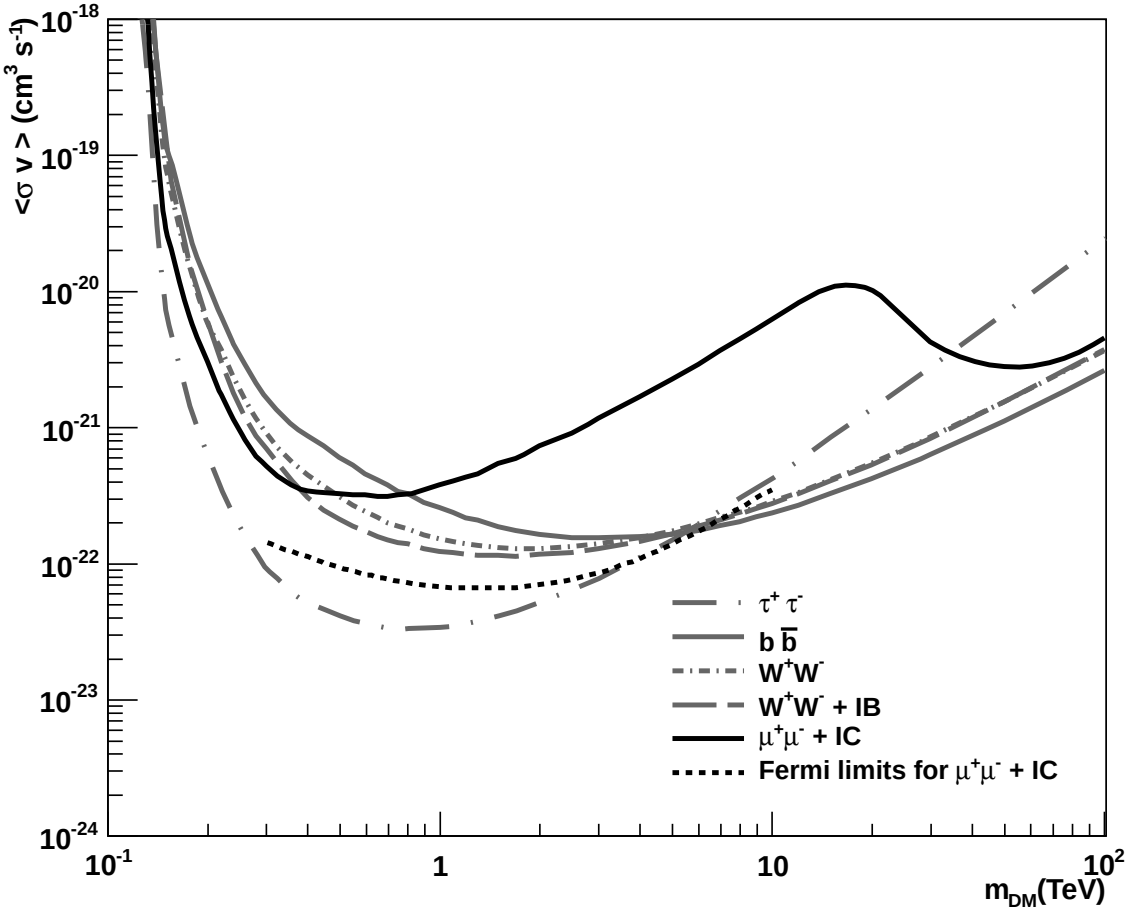

Fig. 7.— The effect of different DM particle models: Upper limit at 95% C.L. on $\langle \sigma v \rangle$ as function of the DM particle mass. The limits are given for $\theta_{\rm max} = 0.1^{\circ}$and the NFW profile RB02. The limits are shown for DM particles annihilating into $b\bar{b}$ (gray solid line) , W^+W^- (gray dash-dotted line), $\tau^+\tau^-$ (gray long-dash-dotted line) pairs. The effect of Internal Bremsstrahlung (IB) occuring for the W^+W^- channel is plotted in gray long-dashed line. The black solid line shows the limits for DM annihilating into $\mu^+\mu^-$ pairs including the effect of inverse Compton (IC) scattering. The *Fermi*-LAT upper limits (Ackermann *et al.* 2010a) for the NFW profile RB02 and for an DM annihilating into $\mu^+\mu^-$ pairs including the effect of IC scattering are also plotted (black dotted line). See section 2.2 for more details.

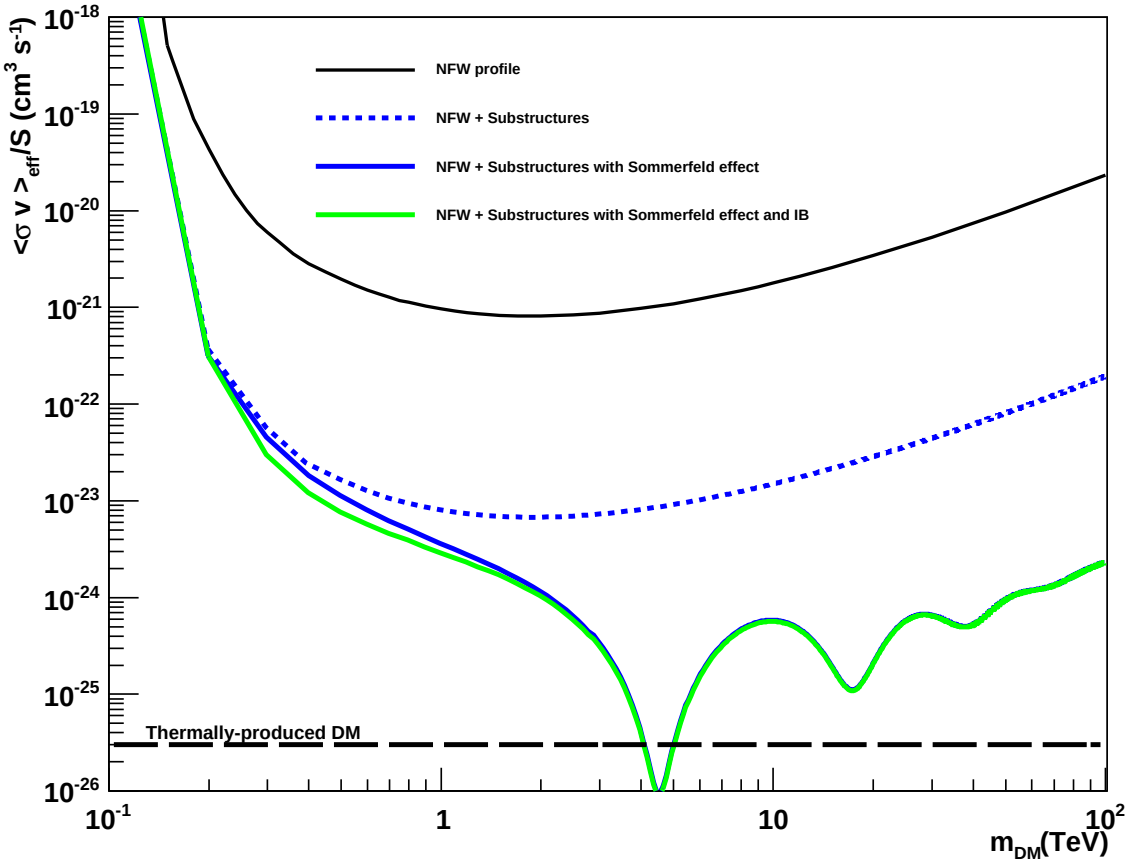

Fig. 8.— The Sommerfeld effect: Upper limits at 95% C.L. on the effective annihilation cross-section $\langle\sigma v\rangle_{\rm eff} = \langle\sigma v\rangle_0 / S$ as a function of the DM particle mass annihilating into W pairs. The black line denotes the cross-section limit for $\theta_{\rm max} = 1.0^\circ$ without γ-ray flux enhancement, the dashed blue line shows the effect of halo substructure (using the "high boost", cf. Fig. 9). The solid green and blue lines show the limit for the case of Wino dark matter annihilation enhanced by the Sommerfeld effect, with and without including Internal Bremsstrahlung, respectively. The DM halo model RB02 is used (see Table 1 and main text for more details). A typical value of the annihilation cross-section for thermally-produced DM is also plotted.

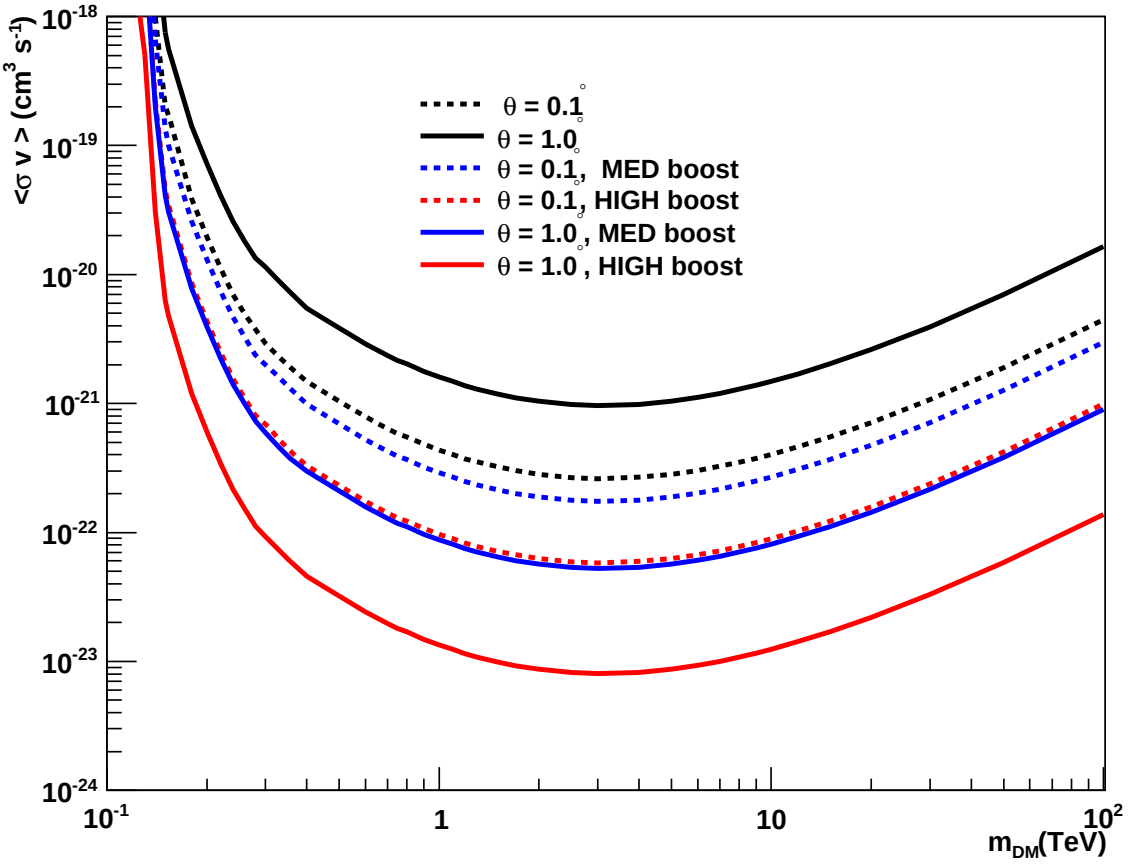

Fig. 9.— The effect of DM halo substructures: Upper limit at 95% C.L. on $\langle \sigma v \rangle$ as function of the DM particle mass annihilating purely into $b\bar{b}$ pairs. The limits are given for $\theta_{\rm max} = 0.1^\circ$ (dashed lines) and $\theta_{\rm max} = 1.0^\circ$ (solid lines). The DM halo model RB02 is used (see Table 1 and main text for more details). In addition, the effect of halo substructures on the $\langle \sigma v \rangle$ limits is plotted. The "medium boost" (MED) with $M_{\rm lim} = 5 \times 10^{-3}$ M$_\odot$ (blue lines) and the "high boost" (HIGH) with $M_{\rm lim} = 10^{-6}$ M$_\odot$ (red lines) are considered.

REFERENCES

Abdo, A. A. *et al.* (2009). (Fermi-LAT Collaboration). *Astrophys. J.*, **707**, 55.

Abramowski, A. *et al.* (2011a). (H.E.S.S. Collaboration). *Astropart. Phys.*, **34**, 608.

Abramowski, A. *et al.* (2011b). (H.E.S.S. Collaboration). *Astrophys.J.*, **735**, 12.

Acciari, V. A. *et al.* (2008). (VERITAS Collaboration). *ApJ*, **679**, 397.

Ackermann, M. *et al.* (2010a). (Fermi-LAT Collaboration). *J. Cosmology Astropart. Phys.*, **5**, 25.

Ackermann, M. *et al.* (2010b). (Fermi-LAT Collaboration). *ApJ*, **717**, L71.

Ackermann, M. *et al.* (2010c). (Fermi-LAT Collaboration). *Phys. Rev.*, **D82**, 092004.

Adriani, O. *et al.* (2009). (PAMELA Collaboration). *Nature*, **458**, 607.

Aharonian, F. *et al.* (2006a). (H.E.S.S. Collaboration). *Science*, **314**, 1424.

Aharonian, F. *et al.* (2006b). (H.E.S.S. Collaboration). *A&A*, **457**, 899.

Aharonian, F. *et al.* (2009a). (H.E.S.S. Collaboration). *A&A*, **495**, 27.

Aharonian, F. *et al.* (2009b). (H.E.S.S. Collaboration). *Astron. Astrophys.*, **508**, 561.

Aharonian, F. A. *et al.* (2009c). (H.E.S.S. Collaboration). *A&A*, **502**, 437.

Aleksić, J. *et al.* (2010a). (MAGIC Collaboration). *ApJ*, **710**, 634.

Aleksić, J. *et al.* (2010b). (MAGIC Collaboration). *ApJ*, **723**, L207.

Arkani-Hamed, N., Finkbeiner, D. P., Slatyer, T. R., and Weiner, N. (2009). *Phys.Rev.*, **D79**, 015014.

Arrenberg, S., Baudis, L., Kong, K., Matchev, K. T., and Yoo, J. (2008). *Phys. Rev. D*, **78**(5), 056002.

Beacom, J. F., Bell, N. F., and Mack, G. D. (2007). *Physical Review Letters*, **99**(23), 231301.

Bergstrom, L. (2000). *Rept. Prog. Phys.*, **63**, 793.

Bergström, L., Bringmann, T., Eriksson, M., and Gustafsson, M. (2005). *Physical Review Letters*, **95**(24), 241301.

Bergström, L., Edsjö, J., and Zaharijas, G. (2009). *Physical Review Letters*, **103**(3), 031103.

Bernlöhr, K. *et al.* (2003). *Astroparticle Physics*, **20**, 111.

Binney, J. and Tremaine, S. (2008). Princeton University Press.

Blasi, P., Gabici, S., and Brunetti, G. (2007). *Int.J.Mod.Phys.*, **A22**, 681.

Bovy, J. (2009). *Phys. Rev. D*, **79**(8), 083539.

Bringmann, T. (2009). *New Journal of Physics*, **11**(10), 105027.

Bringmann, T., Bergstrom, L., and Edsjo, J. (2008). *JHEP*, **01**, 049.

Bringmann, T., Calore, F., Vertongen, G., and Weniger, C. (2011). *Phys. Rev. D*, **84**(10), 103525.

Buote, D. A. *et al.* (2007). *Astrophys. J.*, **664**, 123–134.

Burkert, A. (1996). *IAU Symp.*, **171**, 175.

Chang, J., Adams, J., Ahn, H., Bashindzhagyan, G., Christl, M., *et al.* (2008). *Nature*, **456**, 362.

Cirelli, M., Kadastik, M., Raidal, M., and Strumia, A. (2009). *Nucl.Phys.*, **B813**, 1.

Cirelli, M., Corcella, G., Hektor, A., Hutsi, G., Kadastik, M., *et al.* (2011). *JCAP*, **1103**, 051.

Colafrancesco, S. and Blasi, P. (1998). *Astroparticle Physics*, **9**, 227.

Colafrancesco, S., Profumo, S., and Ullio, P. (2006). *A&A*, **455**, 21.

de Blok, W. J. G. (2010). *Advances in Astronomy*, **2010**.

de Naurois, M. and Rolland, L. (2009). *Astroparticle Physics*, **32**, 231.

Diemand, J., Kuhlen, M., and Madau, P. (2006). *ApJ*, **649**, 1.

Diemand, J., Kuhlen, M., Madau, P., Zemp, M., Moore, B., Potter, D., and Stadel, J. (2008). *Nature*, **454**, 735.

Drinkwater, M. J., Gregg, M. D., and Colless, M. (2001). *ApJ*, **548**, L139.

El-Zant, A., Shlosman, I., and Hoffman, Y. (2001). *ApJ*, **560**, 636.

Feldman, G. J. and Cousins, R. D. (1998). *Phys. Rev. D*, **57**, 3873.

Fukushige, T. and Makino, J. (1997). *ApJ*, **477**, L9.

Griest, K. and Kamionkowski, M. (1990). *Physical Review Letters*, **64**, 615–618.

Hinton, J. A. and Hofmann, W. (2009). *ARA&A*, **47**, 523.

Hinton, J. A., Domainko, W., and Pope, E. C. D. (2007). *MNRAS*, **382**, 466.

Hisano, J., Matsumoto, S., and Nojiri, M. M. (2004). *Physical Review Letters*, **92**(3), 031303.

Jeltema, T. E., Kehayias, J., and Profumo, S. (2009). *Phys. Rev. D*, **80**(2), 023005.

Jungman, G., Kamionkowski, M., and Griest, K. (1996). *Phys. Rep.*, **267**, 195.

Larson, D. *et al.* (2011). *ApJS*, **192**, 16.

Lattanzi, M. and Silk, J. (2009). *Phys. Rev. D*, **79**(8), 083523.

Li, T. and Ma, Y. (1983). *ApJ*, **272**, 317.

Longair, M. S. (1992). *"High Energy Astrophysics: Volume 1, Particles, Photons and their Detection"*. Cambridge University Press.

Mack, G. D., Jacques, T. D., Beacom, J. F., Bell, N. F., and Yüksel, H. (2008). *Phys. Rev. D*, **78**(6), 063542.

McGaugh, S. S. and de Blok, W. J. G. (1998). *ApJ*, **499**, 41.

Mei, S., Blakeslee, J., Cote, P., Tonry, J., West, M. J., *et al.* (2007). *Astrophys.J.*, **655**, 144.

Moore, B., Governato, F., Quinn, T., Stadel, J., and Lake, G. (1998). *ApJ*, **499**, L5.

Moroi, T. and Randall, L. (2000). *Nuclear Physics B*, **570**, 455.

Navarro, J. F. (1998). *astro-ph/9807084*.

Navarro, J. F., Frenk, C. S., and White, S. D. M. (1996). *ApJ*, **462**, 563.

Navarro, J. F., Frenk, C. S., and White, S. D. M. (1997). *Astrophys. J.*, **490**, 493.

Nomura, Y. and Thaler, J. (2009). *Phys.Rev.*, **D79**, 075008.

Paolillo, M., Fabbiano, G., Peres, G., and Kim, D.-W. (2002). *Astrophys.J.*, **565**, 883.

Pedaletti, G., Wagner, S., and Benbow, W. (2008). In *International Cosmic Ray Conference*, volume 3 of *International Cosmic Ray Conference*, page 933.

Pedaletti, G., Wagner, S. J., and Rieger, F. M. (2011). *ApJ*, **738**, 142.

Pfrommer, C., Enßlin, T. A., and Springel, V. (2008). *MNRAS*, **385**, 1211.

Pieri, L., Lattanzi, M., and Silk, J. (2009). *MNRAS*, **399**, 2033.

Pieri, L., Lavalle, J., Bertone, G., and Branchini, E. (2011). *Phys. Rev. D*, **83**(2), 023518.

Pinzke, A. and Pfrommer, C. (2010). *MNRAS*, **409**, 449.

Pinzke, A., Pfrommer, C., and Bergström, L. (2009). *Physical Review Letters*, **103**(18), 181302.

Pinzke, A., Pfrommer, C., and Bergstrom, L. (2011). *Phys.Rev.*, **D84**, 123509.

Profumo, S. (2005). *Phys.Rev.*, **D72**, 103521.

Profumo, S. and Jeltema, T. E. (2009). *J. Cosmology Astropart. Phys.*, **7**, 20.

Reiprich, T. H. and Böhringer, H. (2002). *ApJ*, **567**, 716.

Richtler, T., Schuberth, Y., Hilker, M., Dirsch, B., Bassino, L., and Romanowsky, A. J. (2008). *A&A*, **478**, L23.

Rowell, G. P. (2003). *A&A*, **410**, 389.

Ryu, D., Kang, H., Hallman, E., and Jones, T. W. (2003). *ApJ*, **593**, 599.

Schuberth, Y., Richtler, T., Hilker, M., Dirsch, B., Bassino, L. P., Romanowsky, A. J., and Infante, L. (2010). *A&A*, **513**, A52.

Servant, G. and Tait, T. M. P. (2003). *Nuclear Physics B*, **650**, 391.

Springel, V. *et al.* (2008). *MNRAS*, **391**, 1685.

Tonry, J. L., Dressler, A., Blakeslee, J. P., Ajhar, E. A., Fletcher, A. B., *et al.* (2001). *Astrophys.J.*, **546**, 681.

Voit, G. M. (2005). *Reviews of Modern Physics*, **77**, 207.

Völk, H. J., Aharonian, F. A., and Breitschwerdt, D. (1996). *Space Sci. Rev.*, **75**, 279.